Supporting Information

Kinetic control over self-assembly of semiconductor nanoplatelets

Rebecca Momper[1], Heng Zhang[1], Shuai Chen[1], Henry Halim[1], Ewald Johannes[1], Stoyan Yordanov[1], Daniele Braga[2], Balthasar Blülle[2], David Doblas[3], Tobias Kraus[3,4], Mischa Bonn[1], Hai I. Wang[1] and Andreas Riedinger[1*]

[1]Max-Planck-Institute for Polymer Research, Ackermannweg 10, 55128 Mainz, Germany

[2]Fluxim AG, Katharina-Sulzer-Platz 2, 8400 Winterthur, Switzerland

[3]INM - Leibniz-Institute for New Materials, Campus D2 2, 66123 Saarbrücken, Germany

[4]Colloid and Interface Chemistry, Saarland University, Campus D2 2, 66123 Saarbrücken, Germany

*****Email: riedinger@mpip-mainz.mpg.de

Methods

Characterization. Small Angle X-ray Scattering was performed using a Xeuss 2.0 (Xenocs SA, France) setup equipped with a copper K_α X-ray source emitting at a wavelength of λ = 0.154 nm and a PILATUS 1M (DECTRIS, Switzerland) Hybrid Photon Counting Detector at a sample-to-detector distance of 320 mm by continuously recording 2D diffraction patterns in 15 s intervals until full evaporation of the solvent. Hanging droplets were produced with a NEMESYS computer-controlled pulsation-free syringe pump (Cetoni GmbH, Germany) by pushing the NPL dispersion through a 1 mL glass syringe (Hamilton, USA) that was connected with standard HPLC tubing to a 30 µm-ID fused silica tubing (BGB Analytik Vertrieb GmbH, Germany) as described elsewhere[30]. The 2D scattering patterns were then radially integrated and analyzed using the techniques described previously[30]. Briefly, the liquid volume was calculated from a solvent peak and the agglomerate fraction from the structure factor of the stacked platelets.

For optical spectroscopy, NPL dispersions were transferred to a quartz glass cuvette (10mm). Absorption spectra were recorded on a Cary 60 spectrophotometer. Photoluminescence spectroscopy was recorded using a Prizmatix Silver high power LED (emission peak 369 nm) for excitation and an Avantes SensLine AvaSpec-HSC-TEC for data collection.

Transmission electron microscopy was done using a JEOL1400 microscope (acceleration voltage 120 kV). The samples were deposited on carbon-coated copper grids (400 mesh)

either by drop-casting or self-assembled film deposition. Scanning electron microscopy was performed using either a Hitachi SU8000 or a LEO Gemini 1530 microscope on various substrates (glass, Si wafer, carbon-coated copper grid). Atomic force microscopy was done using a JPK NanoWizard 4 in the AC Mode with a constant amplitude. The used cantilevers (OMCL-AC160TN-R3) were purchased from Olympus with a resonance frequency of 300 kHz and a spring constant of 26 N/m.

Nuclear magnetic resonance spectra were recorded on a Bruker Avance 300 MHz spectrometer with predefined pulse programs. The samples were dispersed in deuterated chloroform, and benzene was added as an internal standard.

Angle-dependent photoluminescence spectra were recorded with the goniometric spectrometer Phelos provided by Fluxim Inc. (Phelos, Fluxim AG, www.fluxim.com). The NPL films were excited with two LEDs emitting at 365 nm over an area of 3x5 mm^2. The measured PL patterns were analyzed using the Emission Module of the simulation software Setfos (Setfos, Fluxim AG, www.fluxim.com).

Micro PL measurements were performed on a commercial setup consisting of an Axiovert 200M inverted microscope and a LSM510 confocal laser scanning unit using a Zeiss Plan-Neofluar 20x NA0.5 microscope objective (all from Carl Zeiss, Jena). Samples were excited at 488 nm (Argon laser), regions of interest were selected and emission spectra were recorded by directing the emitted light to an Andor Shamrock SR-303i-B spectrometer fiber coupled to the LSM 510 module. The spectrometer was equipped with Andor iDus DU420A-OE camera detector and a diffraction grating with 1200 lines/mm (500 nm blaze wavelength), which gave 0.1 nm spectral resolution.

Optical pump-THz probe (OPTP) spectroscopy was employed to investigate the charge states and ultrafast conductivity of photogenerated carriers in NPL dispersion and solids. A laser pulse (400 nm) with ~50 fs duration was used to optically inject electrons into the conduction band, and a THz pulse with 1-2 ps duration was employed as the probe beam. The THz conductivity of photogenerated electrons and holes was measured by recording the pump-induced modulation of the complete THz waveform by electro-optical sampling. See SI for the experimental details.

Chemicals. 1-octadecene (technical grade 90 %, O806-1L) and oleic acid (technical grade 90 %, 364525-1L) were purchased from Aldrich. Selenium powder (200 mesh, 9.999 %) was purchased from Alfa Aesar. Cadmium acetate dihydrate (for analysis, 98 %, 317131000) was purchased from Acros chemicals. N-hexane (≥ 95 %, analytical reagent grade, H/0355/21) and acetonitrile (HPLC grade, A/0626/17) were purchased from Fisher. Acetone (Reah. PhEu, 20066.321) was purchased from VWR chemicals. N-heptane (p.A., K11377279) was

purchased from Merck. N-octane (≥ 99 %, 8753.1) was purchased from Roth. These chemicals were used as received.

Synthesis of Cadmium myristate [Cd(myristate)$_2$]:

Cadmium myristate was synthesized following the procedure described by Rossinelli *et al* [1]. CdO (5.75 g, 44.78 mmol) and 20 mL acetonitrile were mixed in a 100 mL round-bottom flask and stirred at RT (650 rpm). Then, trifluoroacetic acid (0.7 mL, 9.15 mmol) and trifluoroacetic anhydride (6.2 mL, 43.98 mmol) were slowly added. The mixture was stirred for additional 10 min at RT. Afterward, the reaction mixture was heated up to 50 °C under stirring for 1 h. In a 500 mL beaker, 100 mL 2-propanol, triethylamine (14 ml, 100.44 mmol) and myristic acid (10.23 g 44.80 mmol) were combined. The cadmium trifluoroacetate solution was added slowly to the 500 mL baker while stirring. The white precipitate was vacuum-filtered and washed 4 times with 50 mL cold methanol. The final product was collected; dried in a vacuum oven at 40 °C overnight and stored under ambient conditions.

Synthesis of 4 monolayer thick (4 ML) CdSe Nanoplatelets (NPLs):

4 monolayer thick CdSe NPLs were synthesized according to a modified procedure described by Rossinelli *et al.*[1] In a 100 ml three-necked flask, Cd(myristate)$_2$ (170 mg, 0.3 mmol) and selenium powder (12mg, 0.15 mmol) were mixed in 1-octadecene (ODE) (15 mL). The mixture was heated up to 100 °C in 10 min and degassed under vacuum and reflux at 100 °C for 13 min. Under inert atmosphere (argon), the solution was heated up to 240 °C within 16 min. At 188 °C, Cd(ac)$_2$ 2H$_2$O (80 mg, 0.3 mmol) were added quickly. After 6 min at 240 °C, the reaction mixture was quickly cooled down by a water bath. At 185 °C oleic acid (0.5 mL) was added. Then, 5 mL hexane was added and the mixture was centrifuged at 3743 rfc for 5 min. The supernatant was discarded, and the precipitate, containing the 4 ML NPL was redispersed in 5 mL hexane and centrifuged again at 6654 rfc for 5 min. The supernatant, containing the 4 ML NPL, were collected and stored. After a few days, the remaining 3 ML NPLs precipitated from the hexane solution and could be removed by centrifugation at 6654 rfc for 5 min. The remaining 4 ML NPLs in hexane were precipitated using acetone or methyl acetate in a 1:1 volume ratio in order to remove residual ODE and oleic acid. The mixture was stored in the fridge at 5 °C for 1 h hours followed by another centrifugation step at 6654 rfc for 10 min. The precipitate was collected and redispersed in hexane. The dispersed nanoplatelets could be stored in hexane over several months. The purified NPLs were characterized using NMR, optical spectroscopy and TEM.

Self-assembly:

a. Preparation NPL dispersion in different solvents

For the liquid interface self-assembly, the prepared CdSe NPLs were dispersed in either n-hexane, n-heptane or n-octane. Therefore, the solvent of a stock dispersion (nanoplatelets in hexane) was removed using the rotary evaporator and the NPLs were redispersed in the solvent. Afterward, the dispersion was diluted to a certain concentration. The concentration was determined using the lambert beer equation. The molar extinction coefficient of CdSe nanoplatelets could be calculated as described by Yeltik *et al.* [2] The concentration of the NPLs in the dispersion was set between 1.9×10^{-8} M to 4.5×10^{-8} M (concentrations are summed up in Table S1). Only for one experiment a ten times higher concentration of 2.9×10^{-7} M were used. All self-assembly experiments were carried out at 20 °C, except three experiments that were carried out at 5°C in a fridge (see Table S1). The solutions and equipment for the self-assembly experiment at 5 °C were equilibrated for 20 min at 5°C before performing the experiment. For the preparation of the sample for angle-dependent PL and photoconductivity measurements, the materials were equilibrated overnight to avoid thermal gradients and suppress thermally driven flow in solvents to achieve the best long-range ordering.

b. Self-assembly with various solvents and at different temperatures

For the self-assembly experiments, a Teflon well 3.5 cm x 3.5 cm x 3 cm adopted from Gao *et al*.[3] with a cylindrical hole (diameter 1.5 cm) is used (see Figure S1). Inside the hole, a small cylinder is placed as a plateau for the substrate as shown in Figure S1 on the right side. On one side of the well, a small hole is drilled which can be plugged with a rubber plug and a syringe to allow the slow removal of the lower layer. The Teflon well was filled with 2.5 mL acetonitrile and various volumes (tens of µL) of NPL dispersion were added on top. The exact volumes are summed up in Table 1. After addition of the NPL dispersion, the well was covered with a glass petri dish to slow down the evaporation rate of the solvent. After 40 min, the petri dish was removed to allow complete evaporation of the solvent. After additional 20 min, the acetonitrile layer was carefully removed using a syringe plugged in the side of the Teflon well allowing deposition of the formed film on a chosen substrate. During draining, a UV lamp (366 nm) was used to observe the formed film. As substrate carbon-coated copper TEM grids (PLANO, S160-4), silicon wafers (PLANO, G3390-10), or glass were used. The TEM grids and the glass substrates were used without special treatment. The silicon wafers were cleaned with acetone and 2-propanol in the ultrasound bath (10 min) (two times) before use. The obtained films were analyzed by TEM, SEM, and THz spectroscopy.

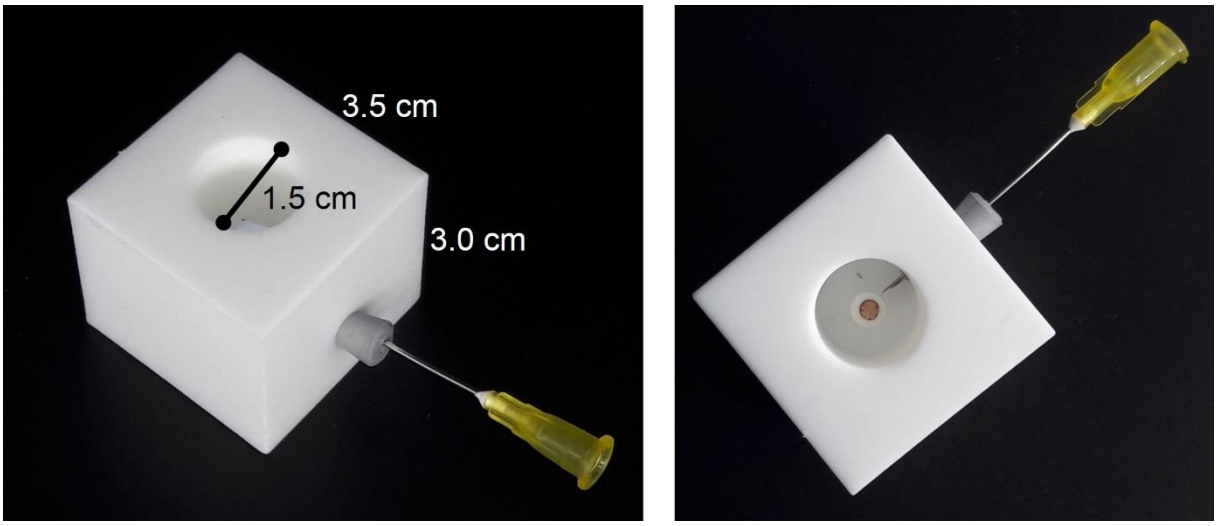

Figure S1: Photograph of the Teflon well with substrate used for self-assembly of NPLs at the liquid interface.

Sample no.	solvent	V/ µL	c/ mol/L	Abs @ 400 nm	T/ °C
SA_1	hexane	60	1.90E-08	0.1663	20
SA_2	hexane	60	2.50E-08	0.1663	5
SA_3	hexane	50	3.60E-08	0.3323	20
SA_4	hexane	60	3.88E-08	0.2761	20
SA_5	hexane	50	3.90E-08	0.3427	20
SA_6	hexane	60	3.90E-08	0.3153	20
SA_7	hexane	50	4.40E-08	0.2615	20
SA_8	heptane	60	2.30E-08	0.1695	20
SA_9	heptane	60	2.60E-08	0.1695	5
SA_10	heptane	70	3.37E-08	0.3323	20
SA_11	heptane	70	3.88E-08	0.2761	20
SA_12	heptane	60	4.18E-08	0.3427	20
SA_13	heptane	50	4.40E-08	0.3293	20
SA_14	heptane	50	4.40E-08	0.3293	20

SA_15	octane	60	1.80E-08	0.1247	20
SA_16	octane	60	1.80E-08	0.1247	5
SA_17	octane	60	3.37E-08	0.3323	20
SA_18	octane	50	4.06E-08	0.2761	20
SA_19	octane	70	4.18E-08	0.3427	20
SA_20	octane	50	4.50E-08	0.2584	20
SA_21	octane	40	2.90E-07	1.9437	20

Table S1: Overview used parameter for self-assembly. Solvent, concentration, volume, and temperature were adjusted to control the orientation of the nanoplatelets at the acetonitrile interface. Absorption values of the respective stock solutions were obtained using a cuvette with 1 cm optical path.

c. Self-assembly in a controlled atmosphere.

In addition to the self-assembly experiments performed in air at 20 °C or 5 °C, the self-assembly experiment was repeated in a closed system to control the alkane vapor content in the atmosphere. The setup shown in Figure S2 were used for the experiment. The Teflon well, where the self-assembly is performed, is placed in a glass evaporation chamber. The chamber is connected to a membrane pump (membrane pump optimal Art.-Nr. 850, Schego), and two flow controllers (Analyt-MTC, Model #: 35829, Messtechnik GmbH & Co KG, Germany). The airflow, generated by the pump, is split and directed into the two flow controllers, regulating the flow. After flow controller 1, a gas washing bottle filled with heptane is placed. The air bubbles through the heptane and enriches the gas phase with heptane. The generated heptane flow is reconnected to the airflow and directed into the evaporation chamber. By varying the flow rates of flow controller 1 and 2, the alkane content in the atmosphere is controlled. For the experiment with no heptane in the atmosphere, the setting for the controllers were 0 (Flow controller 1) and 307 (Flow controller 2). For the experiment with high heptane content in the atmosphere the setting of the controllers were 306 (Flow controller 1) and 6 (Flow controller 2). The temperature was between 21 °C and 22 °C.

To perform the self-experiment, the Teflon well was filled with 2.5 mL acetonitrile and a TEM grid was placed on the small plateau. The evaporation chamber was closed and the air/heptane mixture ran for 20 min through the evaporation chamber. After 20 min, the valves before and behind the evaporation chamber were closed and additional 4 min waited for temperature equilibration. Afterward, 60 µL of the NPLs in heptane ($c=4\cdot10^{-8}$M) was added

using a syringe (Hamilton Gastight #1710, Bonaduz, Switzerland) stick through the septum. After 1 h, the evaporation chamber was opened and the acetonitrile was removed.

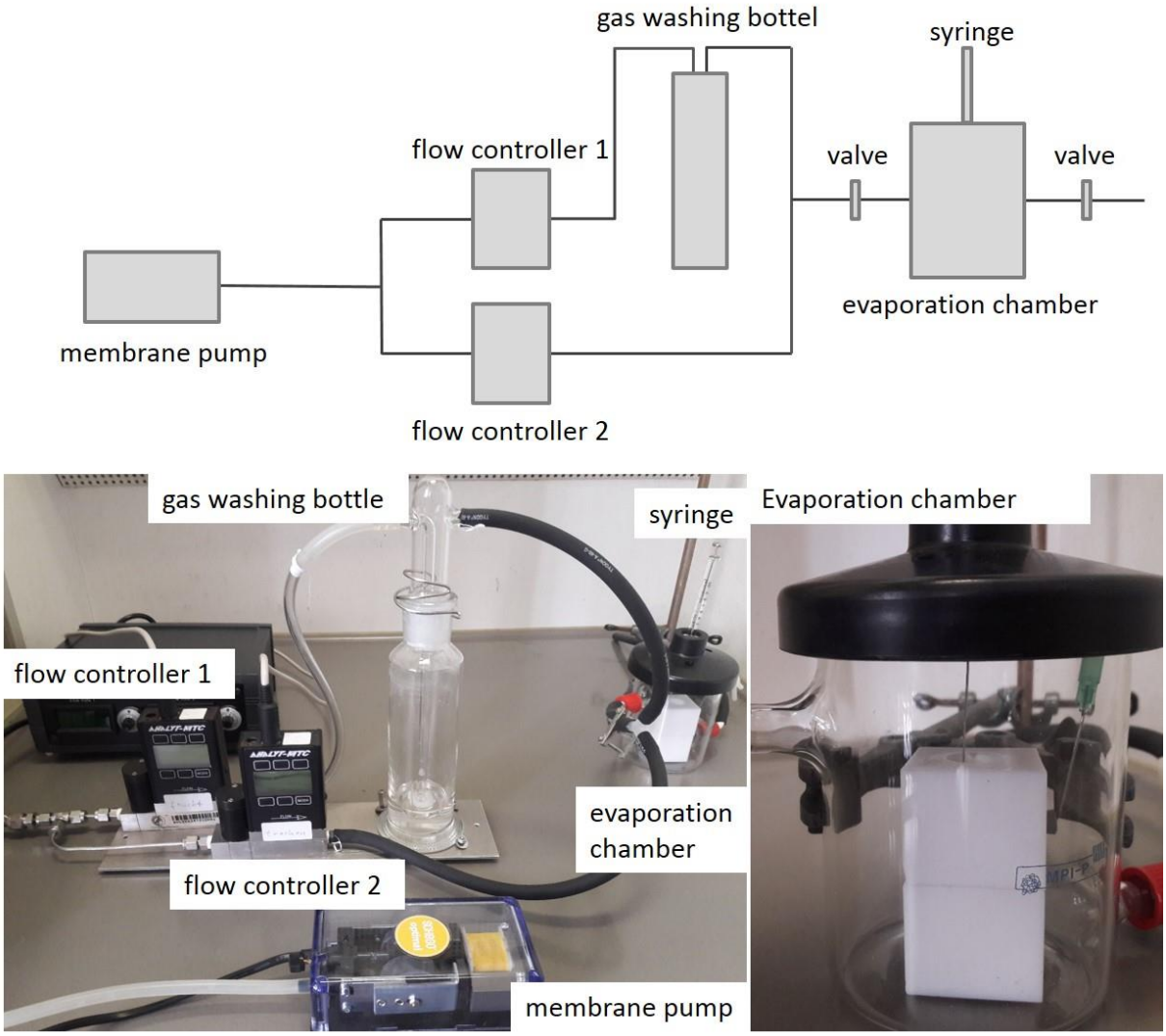

Figure S2: Setup for self-assembly experiment of nanoplatelets under controlled atmosphere. Upper part scheme of the flow setup. Lower part: Photograph of the setup (left) and the evaporation chamber (right).

Determination of 1-octadecene concentration

The concentration of 1-octadecene (ODE), the high-boiling point solvent used during the synthesis, in the purified hexane dispersion were determined using NMR analysis (see Figure S3 a). Benzene was added as an internal standard. The concentration of benzene in the solution analyzed by NMR was set to 1.5 mM. To calculate the concentration of ODE, the ratio of the normalized signal of benzene (blue) and the normalized signal of the double bond of ODE (green) were used (see box in Figure S3 a). The signals were normalized by dividing the integral of the signal by the number of hydrogen atoms related to the signal.

a

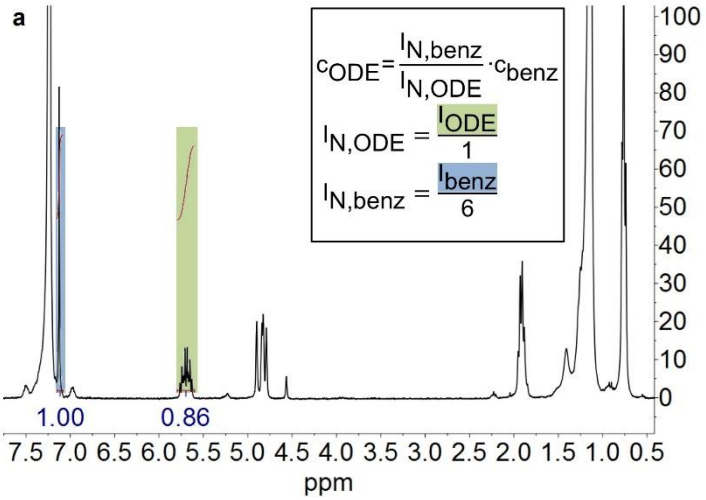

b

sample	c_{ODE}/ mol/L	c_{NPL}/ mol/L	c_{ODE}/c_{NPL}
1	2.90E-03	5.60E-07	5127
2	5.10E-03	3.79E-07	13541
3	2.70E-03	1.08E-06	2503
4	2.70E-03	7.20E-07	3762
5	3.40E-03	1.49E-06	2299

Figure S3: Determination of 1-octadecene content in 4 ML NPL dispersion after normal purification using NMR. a) NMR of 4 ML NPL dispersion with benzene as internal standard (blue), to determine the concentration of 1-octadecene, the equation in the black box was used; b) table summarizing the calculated ODE concentration for different 4 ML NPL samples.

Ligand shell of CdSe NPLs

Since we add oleic acid when cooling down at the end of the synthesis, the surface of the NPLs could be either capped with myristic acid, oleic acid, or a mixture. To elucidate the composition of the ligands present before and after additional purification, the ^{1}H NMR spectra shown in Figure 2 were further analyzed (see Figure S4). In the unpurified sample, a small, broad signal at 5.35 ppm can be found which is attributed to the alkene protons of oleic acid[4] (see Figure S4). A resonance at 0.78 ppm is attributed to methyl protons of oleic, myristic acid, and ODE (see main text for discussion on ODE). For pure oleic acid, the ratio between the integrated intensities of the methyl and alkene resonances should be 1.5 (2 alkene protons and 3 methylene protons). Thus, before thorough purification, oleic acid is present as an impurity. However, after the additional purification step that we perform to remove the ODE the resonance at 5.35 ppm disappears completely, given our signal-to-noise. Thus, our purification protocol efficiently removes both oleic acid and ODE from the NPL dispersions (see red spectra in Figure 2 and Figure S4).

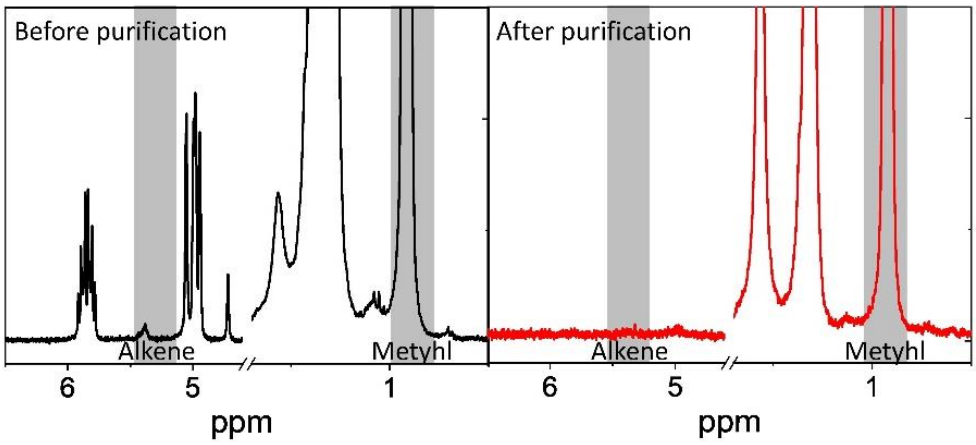

Figure S4: Enlarged ^{1}H NMR spectra of CdSe NPLs to analyze the resonances related to oleic acid. Left: unpurified sample (see black spectra in Figure 2); right: purified sample (see red spectra in Figure 2).

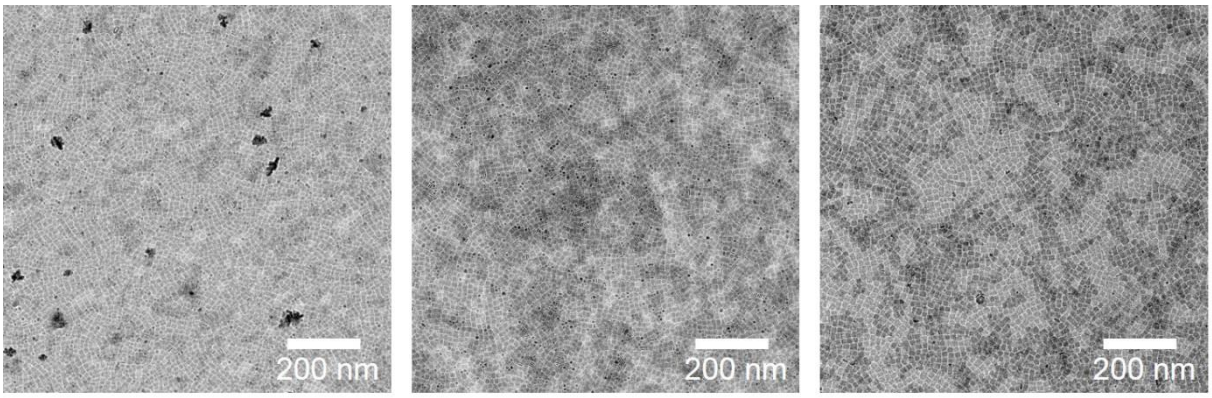

Figure S5: TEM micrographs of 4 ML nanoplatelets further purified (without 1-octadecene) assembled at the acetonitrile interface. Without 1-octadecene, the face-down configuration is reproducibly obtained.

Self-assembly in a controlled atmosphere.

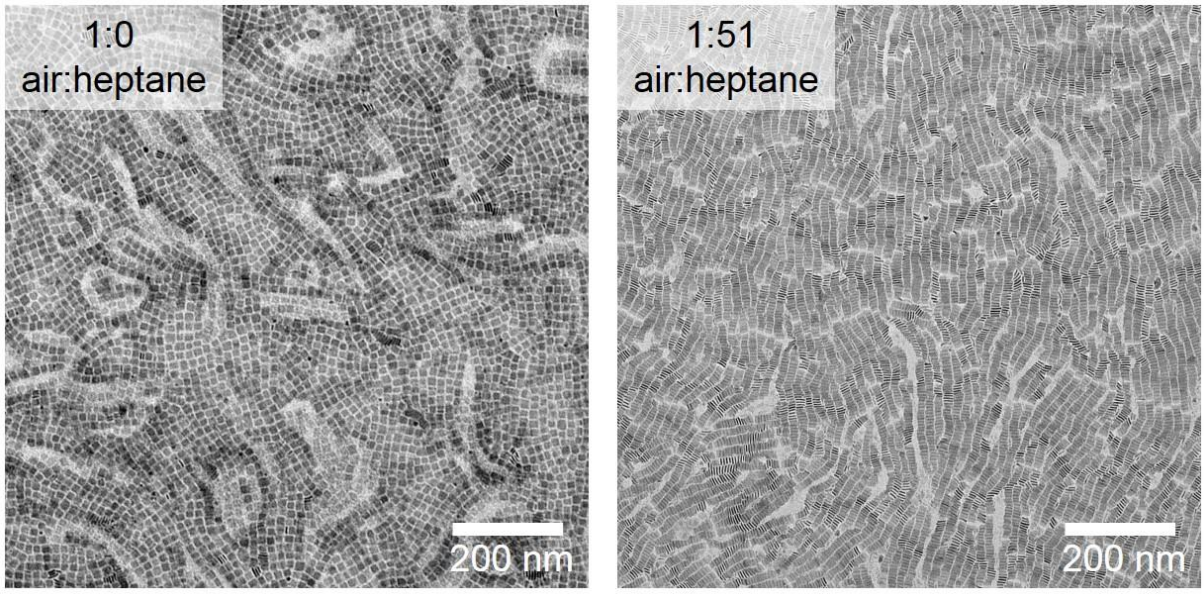

Figure S6: *TEM micrographs of 4 ML NPLs assemblies generated in different atmospheres. Left: Self-assembly performed in the evaporation chamber in air. The NPLs are assembled in the face-down configuration. Right: Self-assembly performed in the evaporation chamber with a high content of heptane in the atmosphere. The evaporation slows down due to the high heptane content and the edge-up configuration is obtained.*

Determination of evaporation rates at 20 °C

We determined the evaporation rate of hexane, heptane and octane under self-assembly conditions we placed a petri dish (5 cm in diameter) on a balance, filled it with 2 mL alkane (hexane, heptane, or octane) and let it evaporate at 20°C and 20% humidity. The weight loss was recorded as a function of time. The slope of linear fit through the origin was divided by the surface area of the petri dish to obtain the evaporation rate normalized per unit of surface area (see below table below).

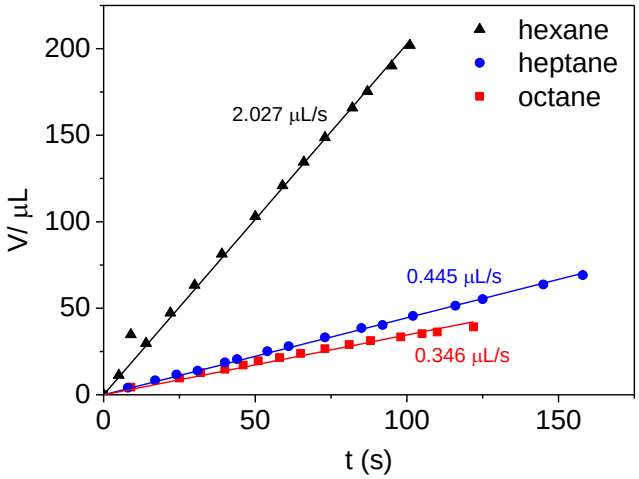

Figure S7: Evaporation rates of hexane, heptane, and octane at 20°C and 20% humidity determined by plotting the weight loss versus time and fitting the data points with a linear function through the origin.

Solvent	Evaporation rate [µL/(s×cm²)]	Time for complete evap. (50 µL) [min]
hexane	0.103	4.6
heptane	0.023	20.5
octane	0.018	26.2

Table S2: Evaporation rate per unit area and calculated time until complete evaporation in a typical self-assembly experiment at 20°C (using 50 µL of NPL dispersion).

Estimation of evaporation rates at 5°C

The flux of evaporating molecules φ per time unit and area unit can be calculated from the Hertz-Knudsen equation where *p* is the pressure, *m* is the mass of one molecule, k_b is the Boltzmann constant, *T* is the temperature, N_a is the Avogadro constant, *R* is the gas constant and α is an evaporation factor [5].

$$\varphi = \frac{\alpha p}{\sqrt{2\pi m k_b T}} = \frac{\alpha p N_A}{\sqrt{2\pi M R T}}$$

$$\rightarrow \alpha = \frac{\sqrt{2\pi M R T}\rho}{\alpha p M}$$

The evaporation factor *α* was calculated by using the experimentally determined evaporation rates at 20 °C and 20 % humidity. Assuming a constant evaporation factor in the applied temperature range (5 °C to 20 °C), the mass flux at 5 °C can be estimated using the following equation where *ρ* is the density of the liquid and *M* the molar mass.

$$\varphi_{vol} = \frac{\alpha p M}{\sqrt{2\pi M R T}\rho}$$

The vapor pressures for the used solvents at 5 °C were calculated using the Antoine equation [6].

Solvent	Evaporation factor	Vapor pressure at 5 °C [Pa]	Evaporation rate at 5 °C [µL cm^{-2} s^{-1}]
hexane	1.8E-05	7866	0.050
heptane	1.3E-05	2052	0.010
octane	3.3E-05	538	0.007

Table S3: Estimated evaporation factor, calculated vapor pressure at 5 °C and calculated evaporation rate per unit area at 5°C

Small-angle X-ray scattering on a hanging droplet

The 2D scattering patterns of a hanging droplet containing an octane NPL dispersion was recorded in a Xeuss 2.0 setup at a sample-to-detector distance of 320 mm during the evaporation of the solvent. The data were radially integrated to obtain 1D curves (see Figure S7). As the concentration is known, and assuming that NPL dispersion is initially fully dispersed and fully agglomerated when the solvent has evaporated, we can follow the rise in the concentration by measuring the liquid volume from the solvent peak, and the agglomerate fraction from the structure factor of the platelets (see Figure S8).

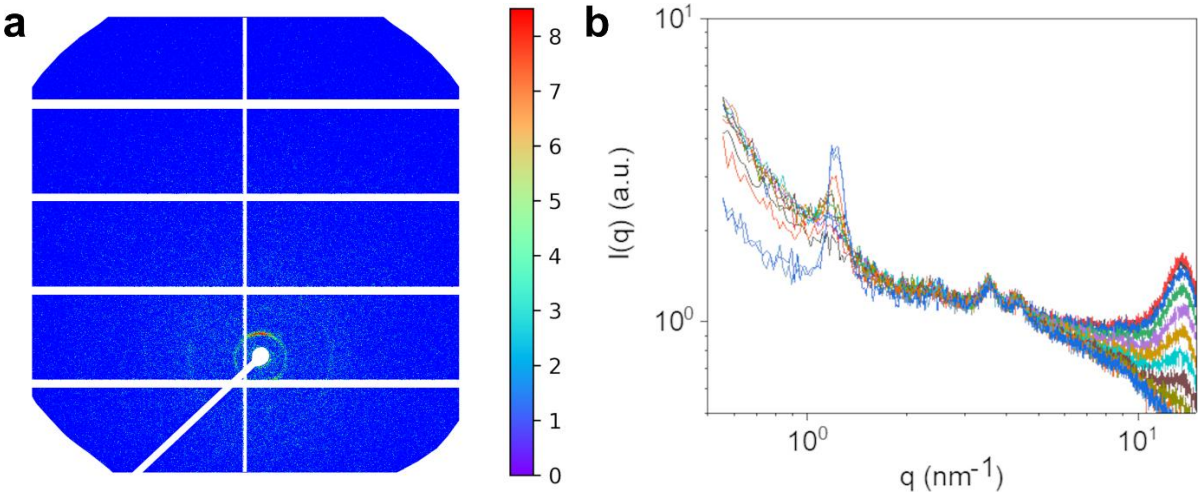

Figure S8: a) Full 2D detector image of a SAXS pattern at the last stage of evaporation of a NPL dispersion in octane at RT. The exposure time was 15 s for each frame. b) Radially integrated scattering intensity from the dried sample of NPL dispersion during the last step of the evaporation process at a time of 300 s.

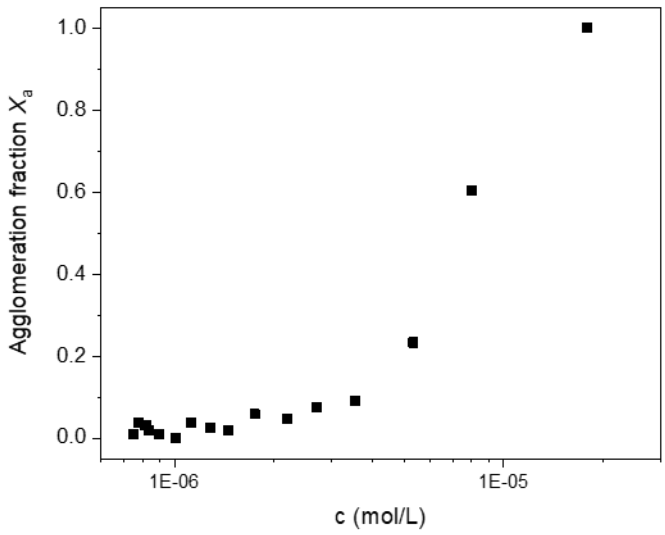

Figure S9: Agglomerate fraction of NPL as a function of NPL concentration in the hanging droplet during evaporation of the solvent.

Determination of height of alkane layer in pendency of concentration and as a function of time

The height of the alkane layer during the self-assembly experiment can be calculated using the following equation with c_{ini} the initial concentration, V_{ini} the initial volume, r the radius of the well and c the current concentration during evaporation. The height of the alkane layer at the critical agglomeration concentration (4.32 E-6 M) is around 3 µm depending on the initial volume (50 µL and 60 µL). The initial concentration was set to 4.14 E- 8 mol/L.

$$h = \frac{c_{ini} \cdot V_{ini}}{c \cdot \pi \cdot r^2}$$

V_{ini} [µL]	c [mol/L)	h [um]
60	4.14E-08	339.53
60	4.32E-06	3.22
50	4.14E-08	282.94
50	4.32E-06	2.69

Table S4: Calculated height of height of alkane layer for at the start of evaporation and at the critical concentration for different volumes

Furthermore, the height of the alkane layer can be determined as a function of time using the calculated evaporation rates by

$$h = \frac{V_{ini} - \frac{\varphi_{vol}}{A} \cdot t}{A}$$

Where V_{ini} is the initial volume, φ_{vol} is the evaporation rate, A is the surface area of the well, and t is the time.

By using the slope of the plot height off alkane layer versus time, the time between reaching the critical agglomeration concentration (2.7 µm height, 50 µL start volume) and complete evaporation can be determined.

Solvent	Temperature [°C]	Slope Evaporation speed [µm s^{-1}]	Time until complete evaporation [s]
hexane	20	-1.03	2.8
hexane	5	- 0.50	5.4
heptane	20	- 0.23	11.7
heptane	5	- 0.18	15.0
octane	20	- 0.10	27.0
octane	5	- 0.07	38.5

Table S 5: Evaporation speed of different solvent for two temperatures (20 °C and 5 °C) and calculated time e from reaching the critical concentration and complete evaporation.

Determination of interparticle distances of the face-down and edge-up configuration

To determine the interparticle distance of NPLs in both configurations, 200 distances for each configuration were measured using the program Image J. A Gaussian fit was used to calculate the mean distance and standard deviation.

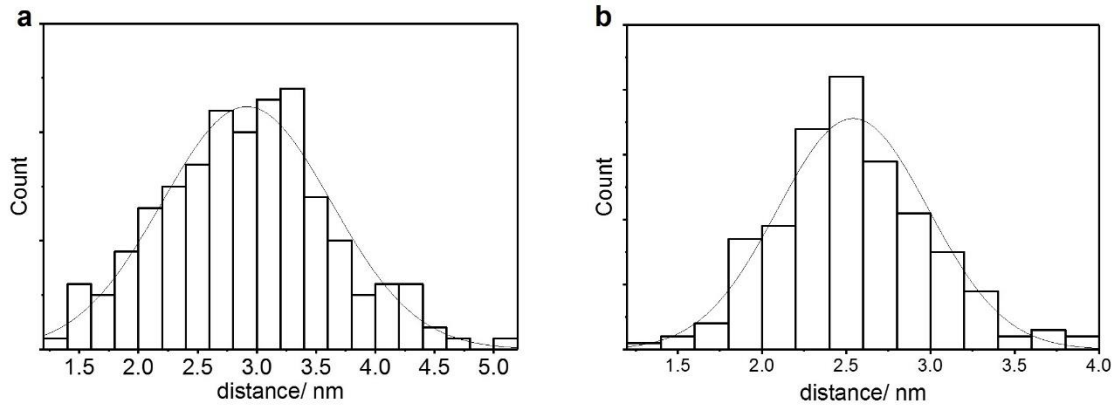

Figure S10: Determination of the interparticle distance of NPL. a) 4 ML NPL assembled in the face-down configuration. The measured mean distance is 2.9 nm; b) 4 ML NPLs assembled in the edge-up configuration. The measured mean distance is 2.5 nm.

Surface coverage of NPL assembly

The theoretical surface coverage *c%* were calculated using an equation with *c* the molar concentration of the NPL dispersion, *V* the used volume, FP_{NPL} the footprint of one NPL in the face-down or edge up configuration, N_A the Avogadro constant and A_{well} the surface area of the well.

$$c\% = \frac{c \cdot V \cdot FP_{NPL,FD\ or\ EU} \cdot N_A}{A_{well}} \cdot 100\%$$

The theoretical surface coverage varied between 77% to 159% for the face-down configuration and 23 % and 243 % for the edge up configuration (see Table S6 and Figure S10). For theoretical surface coverage above 100 %, deposits at the wall of the well were observed.

configuration	Sample no.	c%	configuration	Sample no.	c%
Face down	SA_1	77	Edge up	SA_16	23
	SA_2	102		SA_15	23
	SA_3	122		SA_17	42
	SA_5	133		SA_18	42
	SA_7	149		SA_20	47
	SA_4	158		SA_19	61
	SA_6	159		SA_21	243

Table S6: Calculated theoretical surface coverage for the face-down and edge-up assemblies.

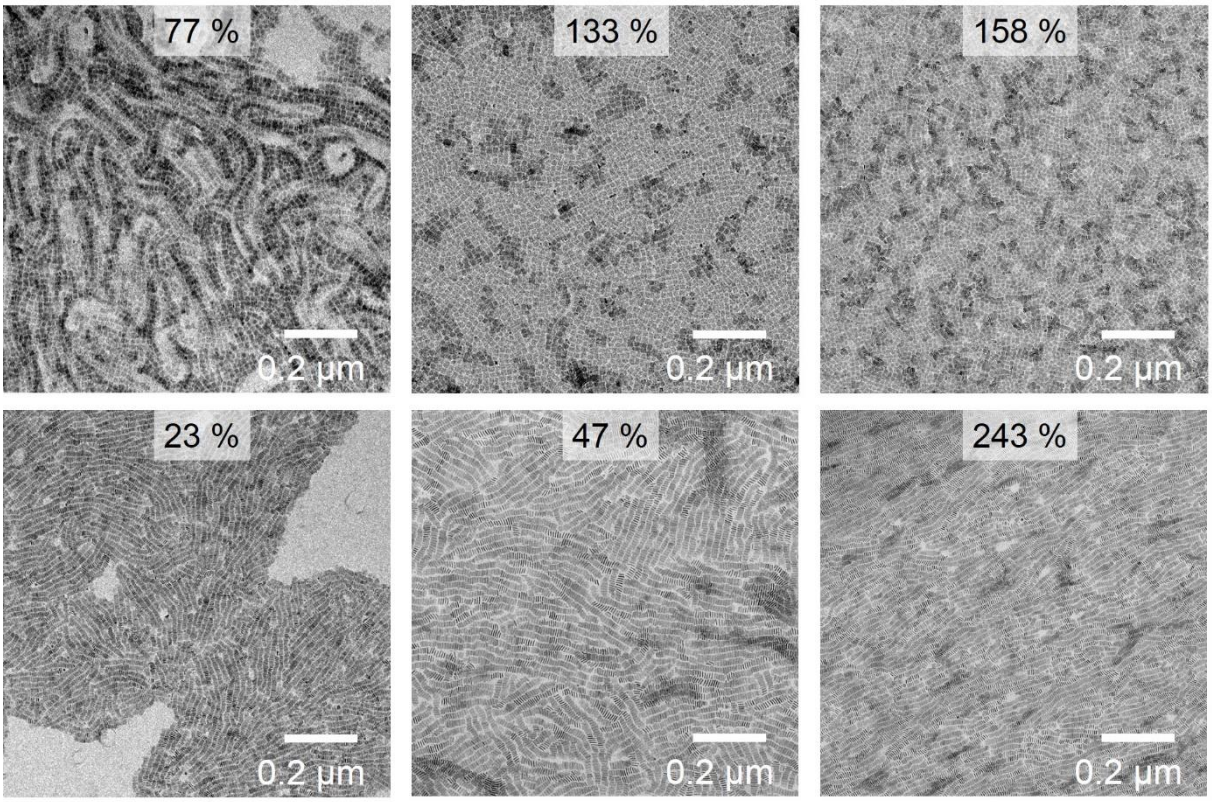

Figure S11: TEM micrographs of 4 ML NPLs assembled in the face-down configuration (upper row) or edge-up configuration (lower row) with varied theoretical surface coverage. Even for lower surface coverage, homogeneous films can be obtained.

Variation of concentration and volume

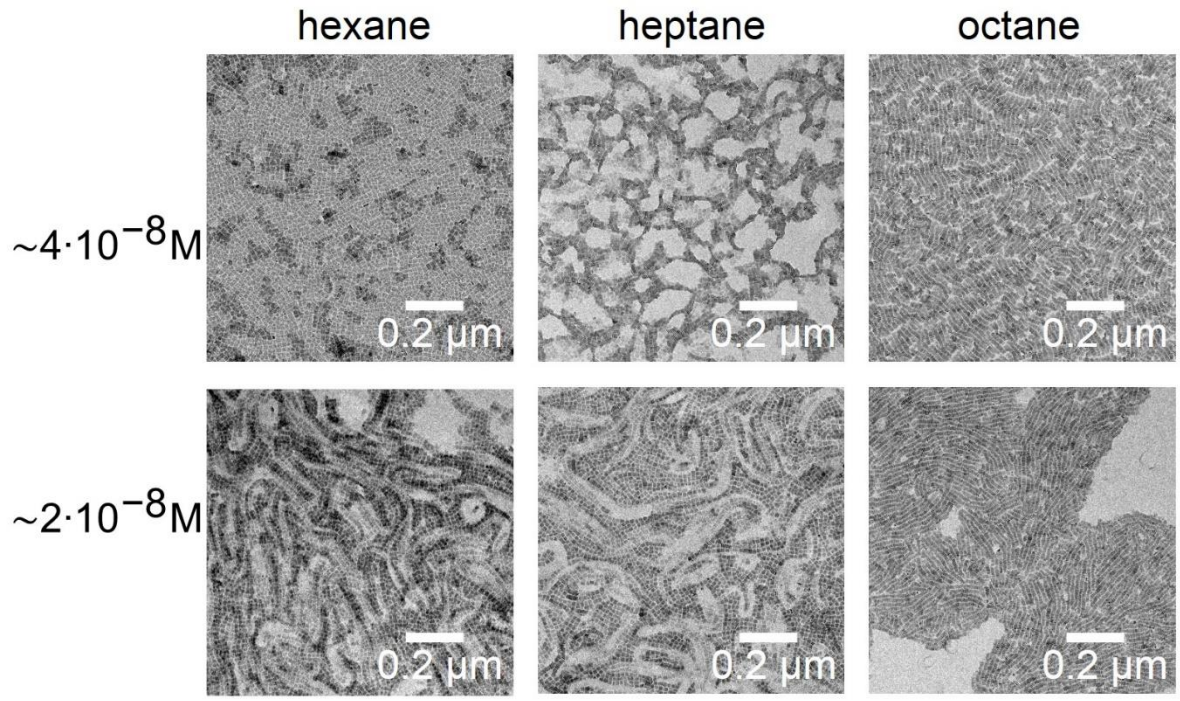

Figure S12: Self-assembly of 4 ML nanoplatelets with varied concentration and constant volume of 50 µL. The self-assembly with half concentrated NPL dispersions leads to the same trend starting from face-down to edge-up by changing the solvent from hexane to octane.

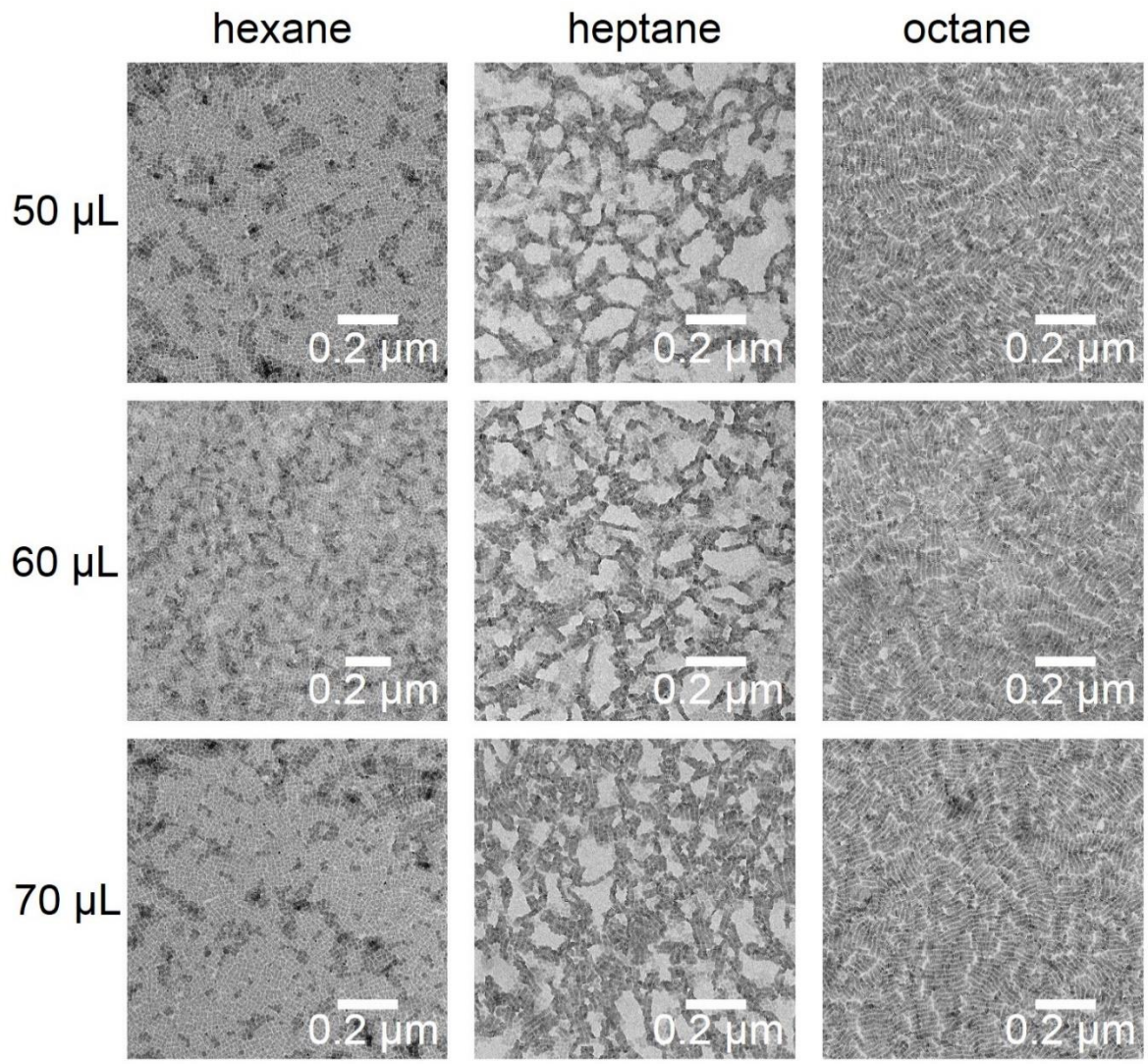

Figure S13: Self-assembly of 4 ML nanoplatelets with a fixed concentration of around $4 \cdot 10^{-8}$ M *and variation of volumes from 50 µL to 70 µL. The same trend from face-down to edge-up by changing the solvent is observed for all volumes.*

Angle-dependent Photoluminescence Spectroscopy

The Photoluminescence (PL) spectrum was measured as a function of emission angle with the goniometric spectrometer Phelos provided by Fluxim Inc. (Phelos, Fluxim AG, www.fluxim.com, see Scheme S1).

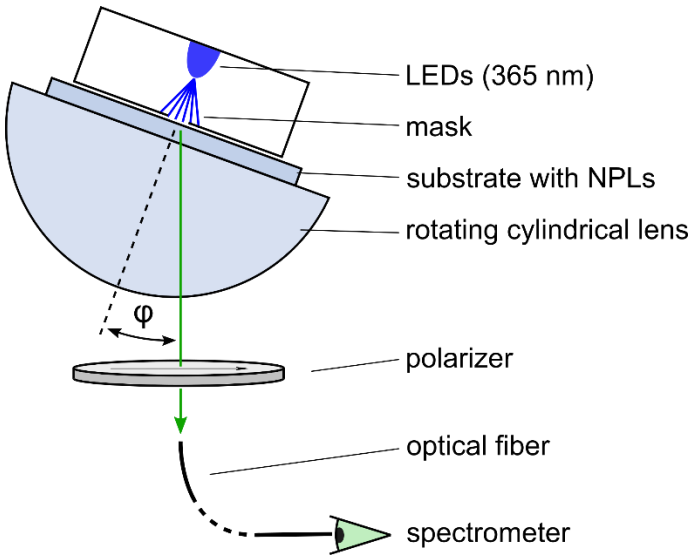

Scheme S1: Schematic illustration of the Phelos goniometric spectrometer. The NPL sample is mounted on a rotating half-cylindrical lens and excited by UV light (365nm). An optical fiber collects the PL signal behind a rotating polarizer.

The samples were mounted on a rotating half-cylindrical lens (BK-7, R = 20 mm), using a refractive index matching fluid (n_D = 1.52, Cargille) to fill the gap between sample and lens surface. The NPL films were excited with a LED emitting at 365 nm over an area of 3x5 mm. Characterizations were performed in both forward and reverse direction, exhibiting low hysteresis and, thus, no sign of degradation upon UV exposure. To reduce stray light, the resulting PL signal was filtered through a pinhole of 1.6x3 mm^2 and collected behind a polarizer by an optical fiber connected to a CCD spectrometer. The angle-dependent PL intensity was obtained by integrating the spectral irradiance (λ_p ~ 515 nm) over the wavelength range of 495 nm to 530 nm.

The measured PL patterns were analyzed using the Emission Module of the simulation software Setfos (Setfos, Fluxim AG, www.fluxim.com), computing the light propagation in a thin film cavity by considering the polarization-dependent Fresnel coefficients of all layer interfaces involved[7-9]. Light emission is modeled by a spatial distribution of radiating electrical dipoles with a dipole moment $\vec{p}$[8, 10, 11]. The average dipole orientation of an ensemble of radiating dipoles can be parametrized by

$$\Theta = \frac{\sum p_z^2}{\sum \vec{p}^2}$$

Where p_x and p_y are the in-plane components parallel to the substrate. Note that Setfos assumes an isotropic distribution within the substrate plane, i.e. $< p_x^2 >=< p_y^2 >$. The average dipole orientation θ in a cavity of a given thickness and refractive index is reflected in a particular angle-dependence of s- and p-polarized PL signal [12].

Only two fitting parameters were used during the simulation, namely, the orientation of the emitting dipoles and the PL intensity. All other parameters, such as the thickness of the emitting layer, the dielectric constant of the CdSe nanoplatelets and the position of the dipole within the emitting layer were kept constant.

Here, the dipole orientation parameter θ was determined by a least-square fit to the measured s- and p-polarized PL patterns, which were normalized to the respective 0° emission beforehand. Thus, the dipole orientation was used Θ as the only fitting parameter, whereas the film thickness was set to d = 4.6 nm, and d = 13 nm, for the face-down and edge-up samples, respectively. The refractive index of the NPL film was estimated as n = 1.63 [3].

Fast Fourier Transformation of TEM micrographs of assemblies in the face-down and edge-up configuration

The program Digital Micrograph GMS3 was used to generate the Fast Fourier Transformation (FFT) of the TEM micrograph of assemblies in both configurations.

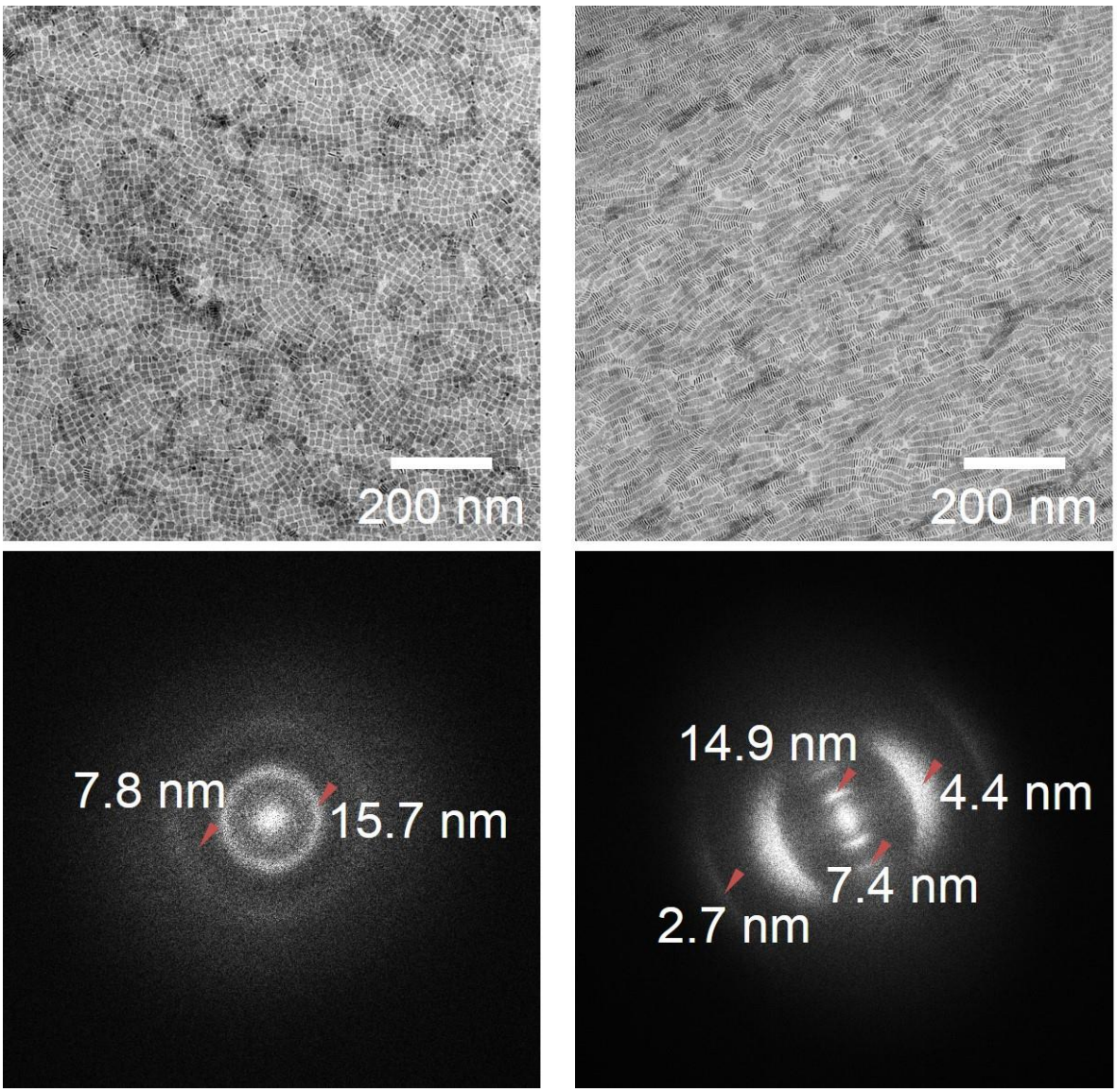

Figure S14: TEM micrograph of NPLs assembled in the face-down configuration (left) and edge-up configuration (right) and the relating FFTs (lower part). The measured distances can be correlated to the interparticle distances of the NPLs. While the face-down assemblies reveal their isotropic orientation by the ring-shaped FFT pattern, a preferential orientation of the stacked NPLs in the edge-up assemblies is evident from the anisotropic structure of the FFT pattern.

Photoluminescence spectra of self-assemblies

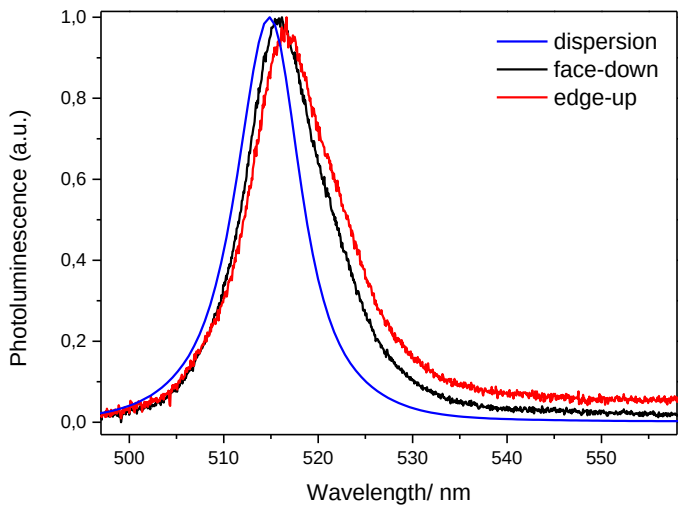

Figure S15: Photoluminescence spectra of 4ML CdSe NPLs in dispersion, in the face-down assembly, and in the edge-up assembly (assemblies on borosilicate glass substrate). The photoluminescence line-width broadens (dispersion < face-down < edge-up) and red-shifts (dispersion < face-down < edge-up) with decreasing distance between NPLs (see Figure S9 and Figure S13).

Sample	Peak wavelength [nm]	FWHM [nm]
Dispersion	**514.73**	**8.08**
Face-down_1	516.45	9.83
Face-down_2	516.59	9.99
Face-down_3	516.60	10.02
Face-down_4	516.60	10.01
Face-down_avg	**516.46±0.07**	**9.96±0.09**
Edge-up_1	517.11	9.86
Edge-up_2	517.14	10.10
Edge-up_3	517.33	10.53
Edge-up_4	517.13	10.10
Edge-up_avg	**517.18±0.10**	**10.14±0.28**

Table S7: Photoluminescence of NPLs in dispersion and in the face-down and the edge-up assemblies. The peak positions and FWHM values were obtained by fitting several photoluminescence spectra with Lorenz functions.

Atomic force microscopy of NPL assemblies on THz glass substrates

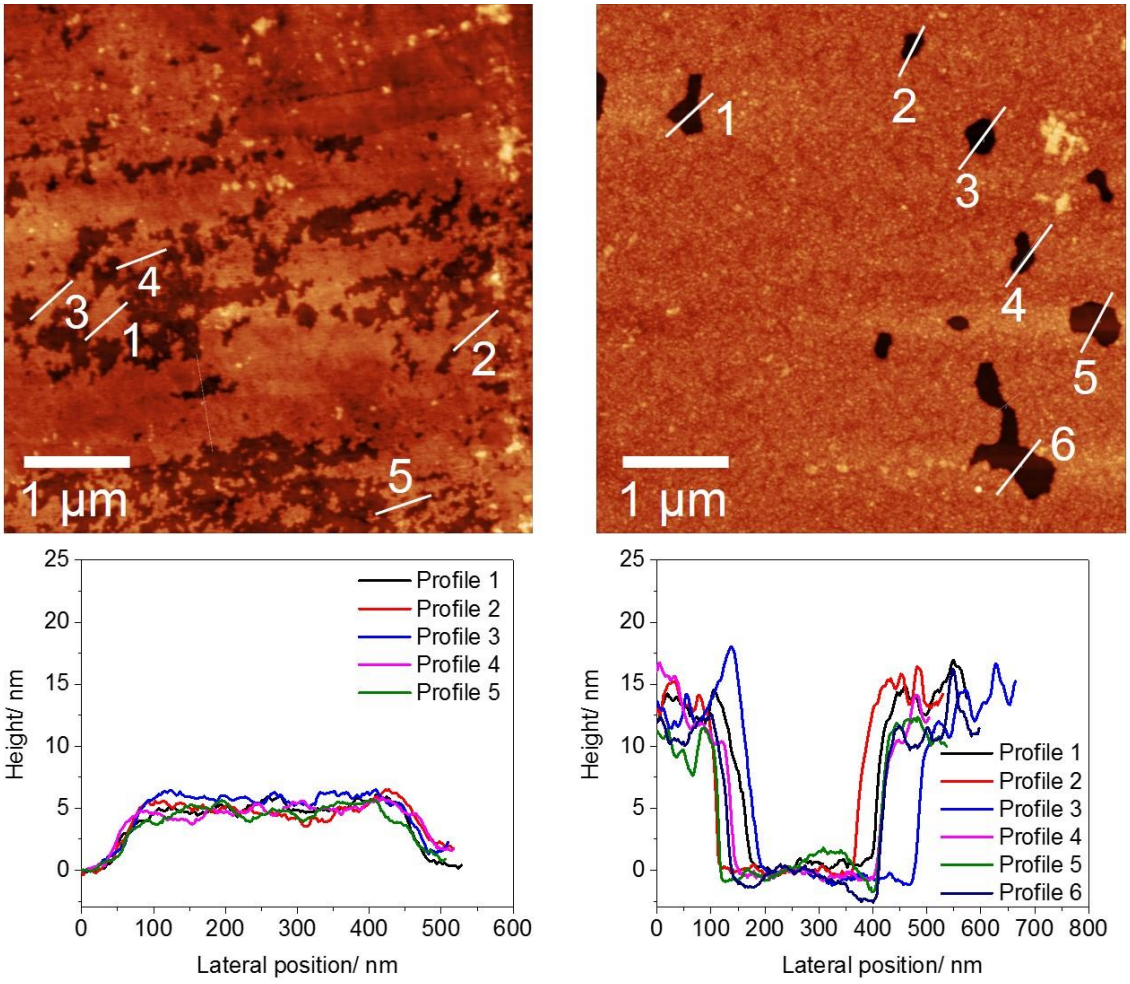

Figure S16: Atomic force microscope images of face-down assembly (left side) and edge-up assembly (right side) transfers to a THz glass slide. Images were taken in the tapping mode at the scan rate of 1 Hz. The raw data were analyzed using the program Gwyddion. For the topographic image, the plane level tool and the align rows tool (polynomial degree 1) was used. The white lines indicate the position of the height profile shown in the lower part. The height of the face-down assembly corresponds to a monolayer of 4ML myristate passivated CdSe NPLs layer flat on the substrate. The height of the edge-up assembly corresponds to a monolayer of 4ML CdSe NPL standing vertically aligned on the substrate.

THz experiments and conductivity dynamics

In this study, optical pump-THz probe (OPTP) spectroscopy is employed to investigate the charge states and ultrafast conductivity of photogenerated carriers in NPL dispersion and solids. In a typical OPTP study, a laser pulse (*e.g.* 400 nm in this study) with ~50 fs duration is used to optically inject electrons into the conduction band, and a THz pulse with 1-2 ps duration is employed as the probe beam. The THz conductivity of photogenerated electrons and holes is measured by recording the pump-induced modulation of the complete THz waveform by electro-optical sampling. When THz wave interacts with free charge carriers in materials, the oscillating electrical field in a single cycle of THz pulse can accelerate the free carriers back and forth within 10s of nanometer spatial range. During this interaction, the THz field is attenuated and the relative THz absorption by free carriers is proportional to their photoconductivity in the materials of interests. On the other hand, in low dimensional (*e.g.* from monolayer to a few layers) semiconducting materials, thanks to the strong quantum confinement and reduced screening effect, the photogenerated electron and hole experience strong Coulomb interactions, resulting in forming strongly bounded electron-hole pair, called exciton. As a charge-neutral quasi-particle, excitons do not absorb THz radiation as free carriers; instead, they induce a pure THz phase shift in the time domain measurements. As the imaginary part of the complex photoconductivity is directly correlated to such phase shift in THz pulse, strongly bounded excitons are typically characterized by an imaginary photoconductivity dominant carrier dynamics, in sharp contrast to a real photoconductivity dominant dynamics for free carriers.

Quantitative analysis of the complex THz Conductivity for excitons and free carriers

(1) Drude-Smith model for describing free carrier conductivity in the edge-up assembly

The Drude-Smith (DS) model[13] is a phenomenological model that describes the transport dynamics of free carriers, in a medium with a preferential charge carrier backscattering process. This is done by introducing the new parameter (so-called c parameter) between 0 and -1 into the classical Drude model. For c=0, the model goes back to the Drude model:

$$\sigma_{DS} = \frac{\varepsilon_0 \omega_p^2 \tau}{1 - i\omega\tau} \times \left(1 + \frac{c}{1 - i\omega\tau}\right)$$

In which ε_0 is the vacuum permittivity, ω_p the plasma frequency and τ the average scattering time. The DS model describes the conductivity of free carriers. The results of D-S model calculations for the edge-up sample are shown in Figure S16a.

(2) The Lorentzian resonance for describing intra-exciton transitions for NPL in dispersion

The exciton resonance in the frequency domain can be described by a Lorentzian resonance originating from, e.g. 1S-2P excitonic transitions by[14, 15]:

$$\sigma(\omega) = \frac{i\omega\varepsilon_0\omega_p^2}{\omega_0^2 - \omega^2 - i\omega\gamma}$$

Where ω_0 is the angular frequency of the oscillatory response and γ defining the width of the resonance.

As two typical examples shown in Figure S16b (with the 1S-2P transitions at 30 and 50 THz), the conductivity can be well fitted by the model, in line with the excitonic nature of the photogenerated species in our NPLs. Unfortunately, due to the very large exciton binding energy in NPL system (over 170 meV)[16], the 1S-2P resonance frequency ω_0 will be accordingly large (> 30 THz, when assuming 170 meV exciton binding energy and hydrogenic Rydberg series of energy levels of the excitonic states in NPLs). Due to the limited bandwidth of the THz spectrometer (up to 2 THz), a simple fit to a Lorentzian lineshape does not allow for the determination of the 1S-2P transition energy of the excitons in the NPLs. Several sets of parameters ω_0, γ yield qualitatively similar fitting results

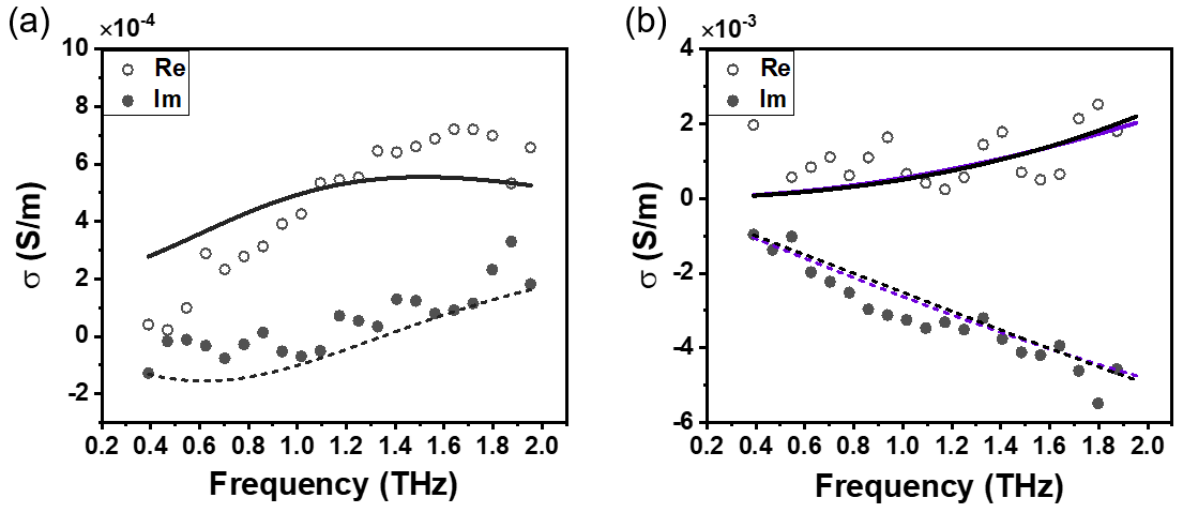

Figure S 17. (a) Drude-Smith fitting for edge-up assembly. The fitting parameters are $\omega_p = 0.04\,THz$, $\tau = 94\,fs$, c=-0.82; (b) Lorentz model fitting for NPL in dispersion. The fitting parameters are $\omega_0 = 50\,THz$, $\gamma = 0.08\,fs^{-1}$, $\omega_p = 0.0035\,THz$ for purple color; $\omega_0 = 30\,THz$, $\gamma = 0.03\,fs^{-1}$, $\omega_p = 0.002\,THz$ for black color.

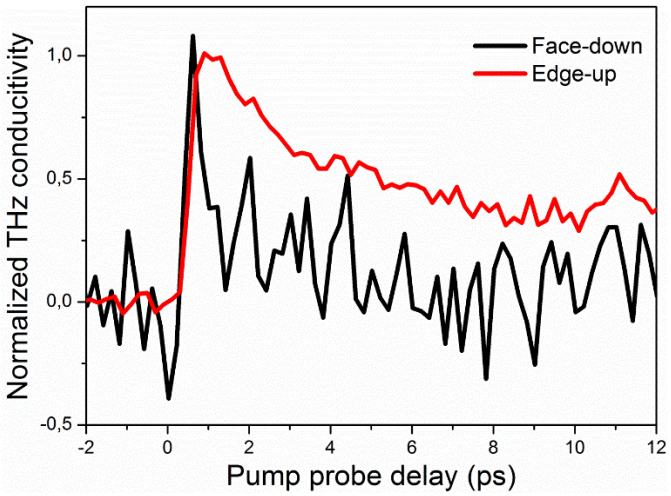

Figure S 18: Normalized, real part of the THz conductivity for edge-up and face-down geometries.

References

1. Rossinelli, A. A.; Riedinger, A.; Marques-Gallego, P.; Knusel, P. N.; Antolinez, F. V.; Norris, D. J. *Chemical Communications* **2017,** 53, (71), 9938-9941.
2. Yeltik, A.; Delikanli, S.; Olutas, M.; Kelestemur, Y.; Guzelturk, B.; Demir, H. V. *The Journal of Physical Chemistry C* **2015,** 119, (47), 26768-26775.
3. Gao, Y.; Weidman, M. C.; Tisdale, W. A. *Nano Letters* **2017,** 17, (6), 3837-3843.
4. Singh, S.; Tomar, R.; ten Brinck, S.; De Roo, J.; Geiregat, P.; Martins, J. C.; Infante, I.; Hens, Z. *Journal of the American Chemical Society* **2018,** 140, (41), 13292-13300.
5. Kolasinski, K. W., *Surface Science: Foundations of Catalysis and Nanoscience Second Edition*. John Wiley & Sons Inc: Chichester, 2009; Vol. 2.
6. Antoine, C. *C. R. Acad. Sci.* **1888,** 107, 681– 684.
7. Sommerfeld, A. *Annalen der Physik* **1914,** 349, (10), 177-202.
8. Neyts, K. A. *J. Opt. Soc. Am. A* **1998,** 15, (4), 962-971.
9. Yeh, P., *Optical Waves in Layered Media*. Wiley-Interscience: 2005.
10. Novotny, L. *J. Opt. Soc. Am. A* **1997,** 14, (1), 91-104.
11. Chance, R. R. P., A.; Silbey, R. , Molecular Fluorescence and Energy Transfer Near Interfaces. In *Advances in Chemical Physics*, 1978; pp 1-65.
12. Schmidt, T. D.; Lampe, T.; Sylvinson, D. M. R.; Djurovich, P. I.; Thompson, M. E.; Brutting, W. *Physical Review Applied* **2017,** 8, (3), 037001.
13. Ulbricht, R.; Hendry, E.; Shan, J.; Heinz, T. F.; Bonn, M. *Reviews of Modern Physics* **2011,** 83, (2), 543-586.
14. Merkl, P.; Mooshammer, F.; Steinleitner, P.; Girnghuber, A.; Lin, K. Q.; Nagler, P.; Holler, J.; Schüller, C.; Lupton, J. M.; Korn, T.; Ovesen, S.; Brem, S.; Malic, E.; Huber, R. *Nature Materials* **2019,** 18, (7), 691-696.
15. Kaindl, R. A.; Carnahan, M. A.; Hägele, D.; Lövenich, R.; Chemla, D. S. *Nature* **2003,** 423, (6941), 734-738.
16. Scott, R.; Achtstein, A. W.; Prudnikau, A. V.; Antanovich, A.; Siebbeles, L. D. A.; Artemyev, M.; Woggon, U. *Nano Letters* **2016,** 16, (10), 6576-6583.